Journal of
Synchrotron Radiation

ISSN 0909-0495

Received 21 August 2008
Accepted 16 January 2009

A new aspect of specific radiation damage: hydrogen abstraction from organic molecules

Alke Meents,[a]* Birger Dittrich[b] and Sascha Gutmann[c]‡

[a]HASYLAB-DESY, Notkestrasse 85, D-22607 Hamburg, Germany, [b]Institut für Anorganische Chemie, Georg August Universität Göttingen, Tammannstrasse 4, D-37077 Göttingen, Germany, and [c]Paul Scherrer Institut, Swiss Light Source, 5232 Villigen, Switzerland.
E-mail: alke.meents@desy.de

Radiation damage is one of the major impediments in obtaining high-resolution structural information utilizing ionizing radiation. From electron microscopy it is known that electron irradiation of biological samples results in the formation of molecular hydrogen. In the present work radiation-induced structural changes of the polypeptide cyclosporine A were observed at a temperature of 100 K. Bond length changes are thought to be due to radiation-induced hydrogen abstraction which chemically modifies the molecules in an irreversible way. The resulting formation of molecular hydrogen might explain the observed increase of the crystal mosaicity, which has also been reported in many previous radiation damage studies.

Keywords: radiation damage; radicals; cryo-crystallography.

1. Introduction

Radiation damage drastically limits the structural information accessible in diffraction experiments with X-rays or electrons. Radiation damage manifests itself in different ways. Loss of contrast, decrease of the diffracted Bragg intensity or $I/\sigma(I)$, unit-cell volume changes, mosaicity and Wilson B-factor increase have all been described in the literature (Teng & Moffat, 2000; Ravelli *et al.*, 2002; Burmeister, 2000; Ravelli & McSweeney, 2000; Weik *et al.*, 2000; Müller *et al.*, 2002). Since these phenomena are not attributed to a certain functional group of a molecule, they are referred to as 'global' radiation damage or 'global non-isomorphism'. Irradiation with X-rays can also induce changes to certain functional groups like cleavage of disulfide bridges or decarboxylation of acidic residues (Burmeister, 2000; Ravelli & McSweeney, 2000; Weik *et al.*, 2000). Since these changes are attributed to a certain functional group, these phenomena are referred to as 'specific' radiation damage. These located changes, which are restricted to a few residues, cannot be solely responsible for the tremendous effects of global radiation damage. Only in one special case could a relation between specific and global radiation damage be found so far. Here glutamic acid is involved in crystal contacts, and radiation-induced decarboxylation of these crystal contacts can explain the unusually high susceptibility of dodecin to radiation damage (Murray *et al.*, 2005). However, a general relationship between specific and global radiation damage has not been found so far.

In cryo-electron microscopy it is well known that intense electron irradiation of biological samples at cryogenic temperatures results in the formation of hydrogen gas (Dubochet, 1988; Leapman & Sun, 1995; Stark *et al.*, 1996; Symons, 1982). The hydrogen bubbles mainly occur in the lipid bilayer of cells (Comolli & Downing, 2005). Comparable observations have been made with X-rays and γ-rays, where the formation of stable carbon radicals owing to radiation-induced hydrogen abstraction is a well known phenomenon (Garrison, 1987; Lamvik *et al.*, 1983). The quantity of carbon radicals formed upon irradiation is directly proportional to the dose.

It was the goal of the present work to determine whether hydrogen abstraction can also be observed in an X-ray diffraction experiment and to identify preferred sites of hydrogen formation in the sample. For this purpose cyclosporine A was chosen as a model system because of its extremely good diffraction properties and its chemical similarity to protein molecules. Cyclosporine A is a cyclic peptide consisting of 11 amino acids (Fig. 1) and diffracts to a resolution of up to 0.62 Å at a temperature of 100 K (Johnas *et al.*, 2009). Refinement at such high resolution yields precise structural information and should allow the identification of small structural changes.

2. Experimental

Orthorhombic cyclosporine crystals were grown by dissolving cyclosporine A at 313 K in PEG 400 and subsequent slow cooling down to room temperature (Giron *et al.*, 1989). Data

‡ Present address: Novartis Institutes for Biomedical Research, Novartis Pharma AG, CH-4056 Basel, Switzerland.

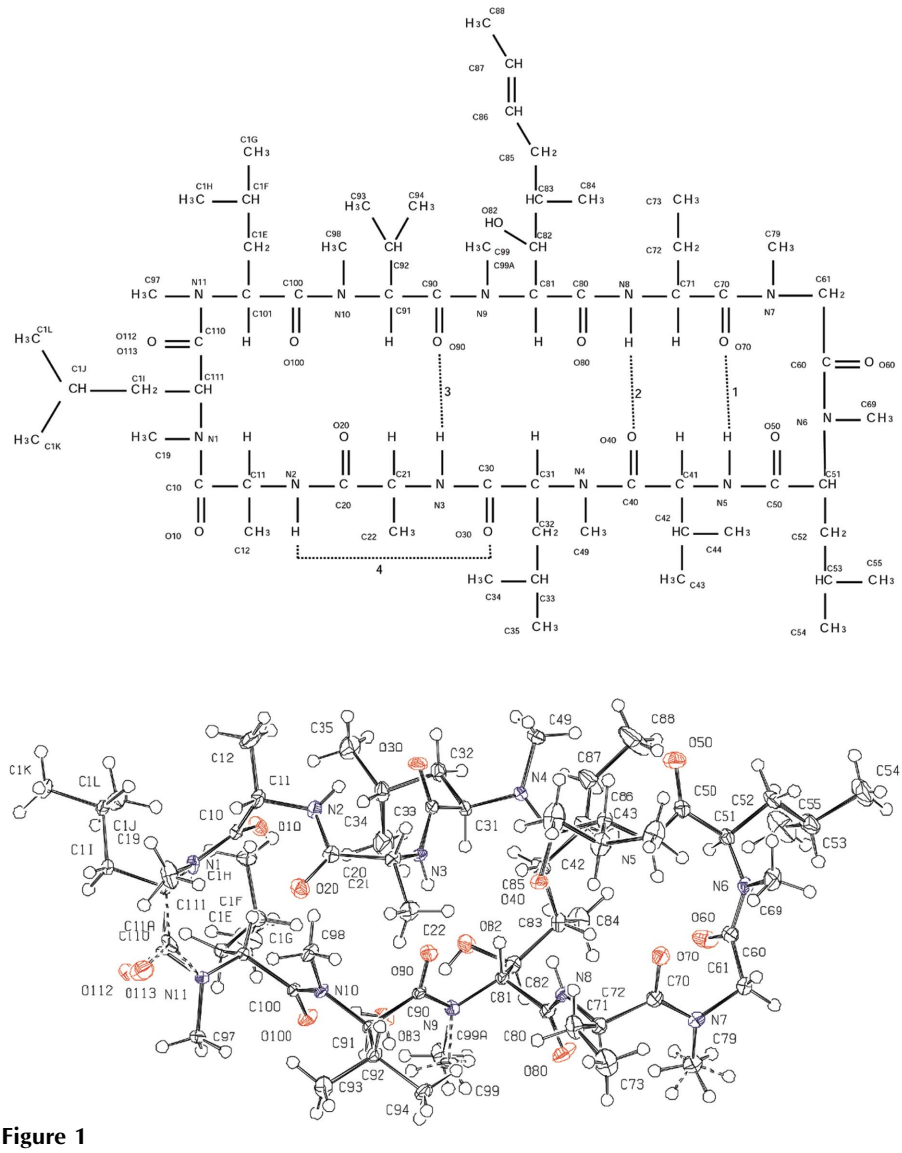

Figure 1
Chemical structure showing (top) intramolecular hydrogen bonding (dotted lines, numbered 1–4) and the atom name convention and (bottom) corresponding *ORTEP* representation of the cyclosporine A molecule.

were collected at the undulator beamline X10SA at the Swiss Light Source at an X-ray energy of 19.5 keV and a temperature of 100 K. The source size at this beamline is 200 × 20 µm [horizontal (h) × vertical (v)] full width at half-maximum (FWHM) and the divergence of the X-ray beam is 150 × 15 µrad (h × v, FWHM). The beam is monochromated using a Si(111) double-crystal monochromator located 19 m downstream from the source. The first monochromator crystal is cryogenically cooled with liquid nitrogen. The second crystal can be sagittally bent for horizontal focusing of the beam. A vertically reflecting and bendable mirror at 19.9 m from the source is used for higher harmonic rejection and vertical focusing. All optical components are located in front of the experimental hutch shutter. Unless the front-end shutter is closed for maintenance reasons, all elements are constantly illuminated by the X-ray beam. Thus no beam-position or wavelength shifts occur owing to thermal load changes on these components when a data collection is started. The sample is located at 23.75 m from the source. The beam size was adjusted to 50 × 150 µm (h × v) for the experiment reported here, resulting in a beam divergence of 600 × 40 µrad (h × v, FWHM). Taking into account the vertical beam divergence, an energy resolution of $\Delta\lambda/\lambda = 1.15 \times 10^{-4}$ and the Bragg angle for the given wavelength, this results in an instrument contribution to the mosaicity of 0.0023° (FWHM).

A prismatic crystal with dimensions of 50 × 70 × 120 µm was chosen for the experiment and flash-cooled in the cryostream to 100 K without any further treatment. During the measurement the crystal was oriented such that the direction of the longest crystal dimension (120 µm) was roughly parallel to the rotation axis with a few degrees of mismatch. With the beam size chosen, the crystal was fully illuminated in its vertical direction perpendicular to the rotation axis by the X-ray beam. This assured a homogeneous irradiation and avoided any systematic error in the results by rotating fresh and unexposed crystal material into the X-ray beam.

During the data collection the incident photon flux was permanently monitored by measuring the current of four PIN diodes arranged around a chromium foil of a few micrometres thickness permanently placed in the monochromatic X-ray beam about 0.5 m upstream of the sample. The signal from this diode arrangement was calibrated to the photon flux by Si pin-diode measurements. Subsequent cross-checking with a calibrated Si diode showed this calibration to be correct within a very few percent (Owen *et al.*, 2009). The automatic conversion of the diode currents to the photon flux is implemented in the beamline software.

The Swiss Light Source is operated in top-up mode (Luedeke, 2004). Thus no intensity decay owing to a decreasing ring current needs to be taken into account. Additionally the X-ray beam position was permanently monitored using a diamond X-ray beam-position monitor (Schulze-Briese *et al.*, 2001). An active feedback system available at the beamline allowed the beam to be kept stable to a position ±1 µm during the experiment.

The incident photon flux dropped only very little over 10.5 h from about 2.7×10^{11} photons s^{-1} to slightly below 2.6×10^{11} photons s^{-1} throughout the experiment, giving an average photon flux of about 2.65×10^{11} photons s^{-1}. For dose

Table 1
Data collection parameters for cyclosporine A at beamline X10SA at the Swiss Light Source.

Energy (keV)	19.5
$\Delta\varphi$ (°)	1
Exposure time (s)	1
Photon flux on sample (photons s^{-1})	2.65×10^{11}
Dose per image (Gy)	6400
Number of images	10800
Detector distance (mm)	100

calculations the geometrical arrangement was simplified by assuming a crystal of 60 × 60 µm thickness and a length of 50 µm (the horizontal beam size) exposed to the X-ray beam. With a Gaussian beam profile in the vertical direction (150 µm FWHM), the crystal was exposed to about 40% of the photons of the full beam. The absorption length for inelastic interactions of 19.5 keV X-rays in cyclosporine A crystal was calculated to be 0.0648 mm^{-1} using the program *XOP* (http://www.esrf.eu/computing/scientific/xop2.1). Combining these parameters with the mass of the irradiated part of the crystal, the absorbed dose in the irradiated volume is about 6400 Gy s^{-1}.

Altogether 10800 images were collected using a Mar 225 mosaic detector with an exposure time of 1 s and a rotation angle of 1° per image. The crystal-to-detector distance was chosen to be 100 mm. In combination with the low wavelength used in the experiment (λ = 0.6360 Å), this allowed the collection of data up to a resolution of d = 0.70 Å without tilting the detector in 2θ. Data collection parameters are summarized in Table 1.

The data were processed in two different dose series of 30 and 60 independently processed data sets using the *XDS* program package (Kabsch, 1993). The first series contained full crystal rotation of 360 images and the second ones half crystal rotations of 180 images. Most of the data analysis was carried out on the series containing the full crystal rotations of 360°; only the mosaicity values were also analyzed from the 180° data. Using full crystal rotations should prevent any effects due to non-uniform irradiation of the crystal and yield better statistics for the subsequent structure refinements. Lattice parameters such as unit-cell volume and crystal mosaicity and the $I/\sigma(I)$ ratios for certain resolution shells were also determined using *XDS*. Relative *B*-factors were refined for all the individual data sets of the dose series by merging all data sets using *XSCALE*. The relative *B*-factor in *XSCALE* is defined as

$$I(\theta)_{\rm scaled} = K\, I(\theta)_{\rm meas} \exp\left[-2B\left(\frac{\sin\theta}{\lambda}\right)^2\right],$$

where K is an individual scale factor for every single data set. The correlation coefficients (cc_F) between the first and the subsequent data sets, consisting of the reflection sets F_h^1 and F_h^2, respectively, were taken as a further indicator of radiation damage. It is routinely determined by *XSCALE* and defined as

$$cc_F = \frac{\sum_h F_h^1 F_h^2 - \sum_h F_h^1 \sum_h F_h^2/N}{\left\{\left[\sum_h \left(F_h^1\right)^2 - \left(\sum_h F_h^1\right)^2/N\right]\left[\sum_h \left(F_h^2\right)^2 - \left(\sum_h F_h^2\right)^2/N\right]\right\}^{1/2}}$$

with N being the number of reflections (Tong, 2001). The mean intensity per data set was also taken from data processing with *XSCALE*.

For all 30 data sets individual structures were refined using *SHELXL* (Sheldrick, 2008). The structure described by Johnas *et al.* (2009) served as a starting model. To avoid any local minima and systematic errors, the same starting file containing the same atomic coordinates was used for all the refinements. Only the lattice parameters were individually adjusted to the values obtained from the *XDS* data processing. For every data set 20 cycles of full matrix least-squares refinements were carried out. All the atomic coordinates of the non-H atoms were freely refined with anisotropic displacement parameters. H atoms were refined in a riding model with isotropic thermal displacement parameters. The crystal structure contains one partly occupied solvent water molecule in its asymmetric unit with a refined occupancy of 0.685 (7). This corresponds to a solvent content of 1%. Positional disorder of atom O112 and methyl group C99 (including its three H atoms) and rotational disorder of the methyl group C79 were taken into account by refining two split positions each. Despite this, no further restraints and constraints had to be applied and for all 30 data sets a stable refinement could be obtained. The lattice and further structure refinement parameters for the first and last data sets are summarized in Table 2.

3. Results

Global radiation damage was followed by a careful inspection of changes of the unit-cell dimensions, crystal mosaicity, lattice strain, relative *B*-factors, mean Bragg intensity, $I/\sigma(I)$ ratio and *R*-factors from the structure refinements. In addition, bond distances and angles as obtained from the structure refinements were analyzed as a function of dose to identify any specific structural changes of the molecule.

3.1. Lattice parameter and relative *B*-factor changes

Fig. 2 shows the changes of different lattice parameters as a function of dose. The unit-cell volume increases in a linear fashion with dose (Fig. 2*a*) with a slightly more pronounced increase at lower doses. A different behaviour is observed for the crystal mosaicity, which first increases in a linear fashion from 0.184° to 0.229° at a dose of 18.4 MGy for 360° processing and from 0.16° to 0.225° at a dose of about 30 MGy for 180° processing and remains in both cases almost constant afterwards up to 69.1 MGy (Fig. 2*b*). The relative *B*-factors refined for each of the 30 different data sets (by scaling with *XSCALE*) show a slightly more pronounced increase at lower doses up to 9.2 MGy and afterwards a linear increase with dose (Fig. 2*c*).

Table 2
Data set and structure refinement parameters of the first, a middle, and the last data set in the dose series of a cyclosporine A crystal.

	Data set number		
	1	15	30
Total dose (MGy)	2.3	34.5	69.1
Empirical formula	$C_{62}H_{111}N_{11}O_{12}\cdot0.685H_2O$	$C_{62}H_{111}N_{11}O_{12}\cdot0.658H_2O$	$C_{62}H_{111}N_{11}O_{12}\cdot0.602H_2O$
Formula weight (g mol^{-1})	1216.3	1216.3	1216.3
Cell setting	Orthorhombic	Orthorhombic	Orthorhombic
Space group, Z	$P2_12_12_1$, 4	$P2_12_12_1$, 4	$P2_12_12_1$, 4
Temperature (K)	100	100	100
Unit-cell dimensions			
a (Å)	12.510	12.510	12.509
b (Å)	15.643	15.648	15.652
c (Å)	35.748	35.810	35.859
$\alpha = \beta = \gamma$	90	90	90
V (Å^3)	6995.7	7010.0	7020.9
Calculated density (g cm^{-3})	1.155	1.152	1.151
$F(000)$	2654	2654	2654
Crystal size (mm)	0.05 × 0.07 × 0.12	0.05 × 0.07 × 0.12	0.05 × 0.07 × 0.12
Crystal form, colour	Rectangular, colourless	Rectangular, colourless	Rectangular, colourless
Wavelength λ (Å)	0.6360	0.6360	0.6360
Absorption coefficient, μ (mm^{-1})	0.081	0.081	0.081
Absorption correction	None	None	None
Maximum θ (°)	28.38	28.38	28.35
No. of measured reflections	126082	128250	132836
No. of independent reflections	11255	11449	11520
No. of observed reflections [$I > 2\sigma(I)$]	11060	11109	10734
R_{merge}	0.013	0.020	0.033
$I/\sigma(I)$ (0.7–15.65 Å)	64.0	45.1	35.9
$I/\sigma(I)$ (0.7–0.8 Å)	40.0	26.3	15.6
R [$F^2 > 2\sigma(F^2)$]	0.0356	0.0540	0.073
$wR(F^2)$	0.0938	0.1441	0.1805
No. of parameters	950	950	950
No. of restraints	12	12	12
S	1.071	1.504	1.709
$\Delta\rho_{max}$ (e Å^{-3})	0.292	0.352	0.386
$\Delta\rho_{min}$ (e Å^{-3})	−0.175	−0.255	−0.287

3.2. Intensity decay

The intensity decay of the recorded Bragg reflections was analyzed in two different ways. The decrease of the $I/\sigma(I)$ ratio in the outermost resolution shell (0.7–0.8 Å) with dose is shown in Fig. 3(*a*). The graph clearly follows an exponential decay function. Analysis of the $I/\sigma(I)$ ratio has the disadvantage that it is not only sensitive to the decay of the diffracted intensities I, but also takes into account an increase of $\sigma(I)$ owing to larger integration box sizes and an increased background level as a result of radiation-induced disorder in the crystal. Another indicator of the radiation-induced intensity decay is the mean diffracted intensity per data set (resolution range 0.7–15.65 Å) as a function of dose as shown in Fig. 3(*b*). At doses up to 11.5 MGy the mean intensity decays rapidly and at higher doses more slowly. As already observed for the $I/\sigma(I)$ ratio, the decay is well described using an exponential decay function. A more or less linear dependence with a slightly more emphasized decay for doses above 35 MGy is observed for the decay of the correlation coefficient between the first and the subsequent data sets with dose (Fig. 3*c*). Whereas the decay of the diffracted Bragg intensities is mainly dominated by the integrity of the crystalline lattice, the correlation coefficient is a measure for the integrity of the structural motif, *i.e.* the molecule itself. The $R1$ value ($R1 = \Sigma||F_o| - |F_c||/\Sigma|F_o|$) of the structure refinement increases almost linearly with dose (Fig. 3*d*) with a slightly stronger increase at lower doses.

3.3. Molecular changes

By comparing the first and the last structure of the dose series, apparent bond length changes could be observed. Changes in the bond distance between the first and the last data set (larger in magnitude than 0.0045 Å) are shown in Fig. 4. The largest apparent bond-length change is observed for the double bond between the C86 and C87 atoms. The refined bond length decreases in a linear fashion from 1.309 (2) to 1.272 (6) Å (Fig. 5*a*). This bond-length contraction by 0.037 Å is 18.5 times the value of the initial standard deviation of 0.002 Å and can therefore be considered to be significant. Owing to the radiation-damage-induced loss of high-resolution scattering power, the $I/\sigma(I)$ ratio in the outermost shell (0.7–0.8 Å) decreases from 40.0 to 15.6 (Fig. 3*a*), which is still a good signal-to-noise ratio. However, this loss of information results in an increase in the standard deviations of the bond lengths with dose.

Further bond contractions are observed for most of the carbonyl bonds (C═O) in the peptide backbone. The C═O bonds also contract linearly with dose and the bonds contract by up to 0.017 Å (Fig. 5*b*). The chemical bonds forming the backbone show a diverse behaviour. Some of the chemical bonds expand slightly, for example some C—C bonds (Fig. 5*c*), whereas others show both an elongation and contraction at different places (C—N bonds, Fig. 4). Most of the C atoms bound to an α-C of the peptide backbone show a slight bond elongation. Only in the case of one alanine residue (C11, Fig. 4) is a C—C bond contraction observed.

In the aliphatic side chains most of the tertiary C atoms carrying a H atom show a contraction of the bond length (Figs. 4 and 5*d*). In the case of two methyl groups bound to a tertiary C atom, the bond contraction to one methyl group systematically accompanies an elongation of the chemical bond to the other methyl group (Fig. 5*d*). Interestingly in this

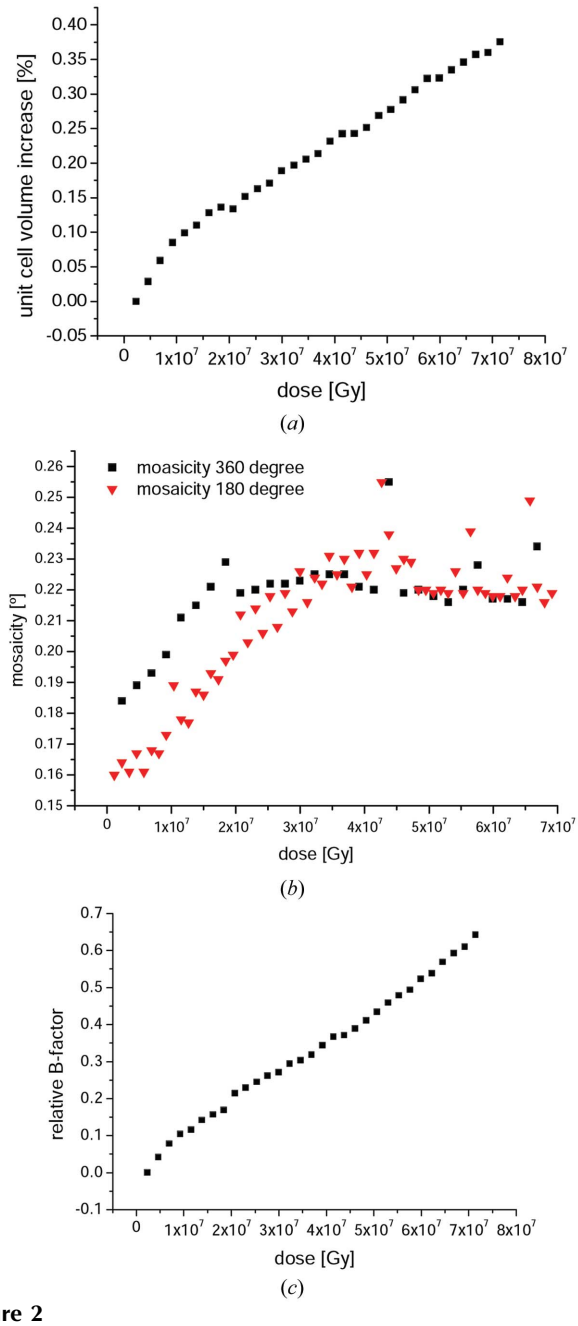

Figure 2
Lattice parameter changes as a function of dose. (*a*) Unit-cell volume changes. (*b*) Crystal mosaicity changes for full rotation (squares) and half crystal rotation (circles) data sets. (*c*) Relative *B*-factor increase as obtained from scaling with *XSCALE*.

case the contraction is observed for the initially shorter bond, whereas the initially longer bond slightly elongates.

Fig. 6 shows the thermal displacement ellipsoids (50% probability level) for C86, C87 and their neighbouring atoms, illustrating the increase of the ellipsoids of the anisotropic displacement parameters. In contrast to the bond-length changes, no significant bond-angle changes were observed. Analysis of the thermal displacement parameters for the H atoms did not yield any clear and significant results.

In the present work radiation-induced structural changes are modelled by refining the atomic positions together with

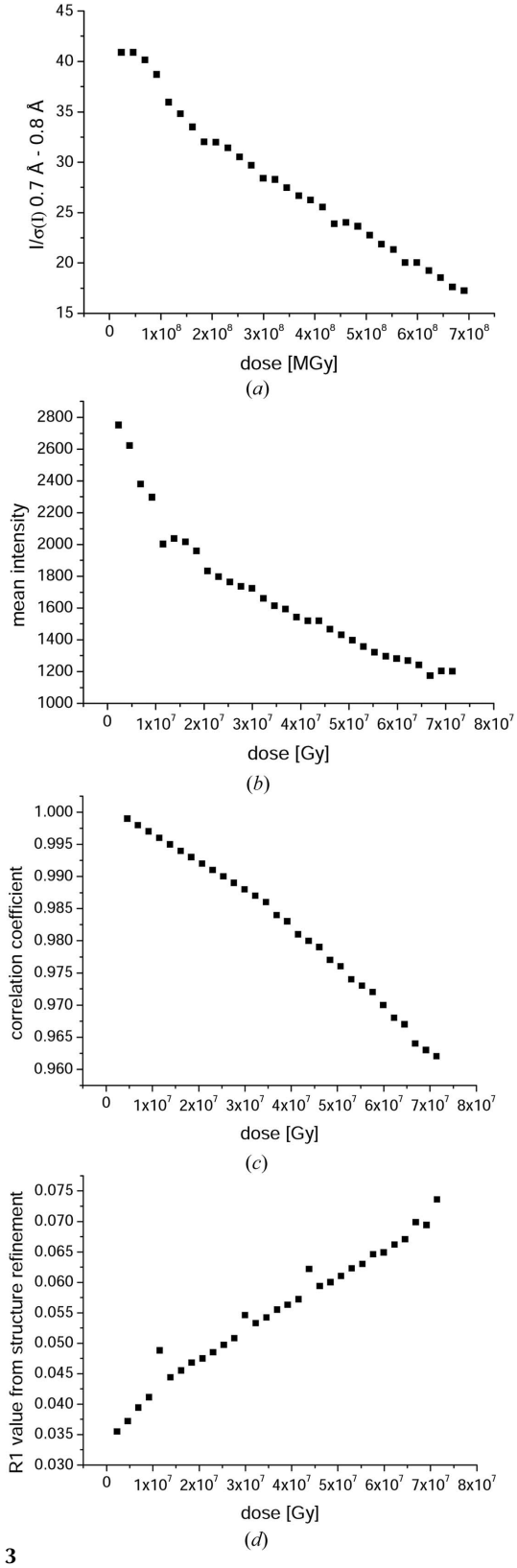

Figure 3
Bragg intensity decay and further indicators for radiation damage as a function of dose. (*a*) Changes of the mean $I/\sigma(I)$ ratios for $I > 2\sigma(I)$ in the 0.7–0.8 Å resolution shell. (*b*) Mean Bragg intensity per data set (resolution range 0.7–15.65 Å). (*c*) Changes of the correlation coefficients between the first and the following data sets. (*d*) Changes of the *R*1 values ($R1 = \Sigma||F_o| - |F_c||/\Sigma|F_o|$) from the structure refinement with *SHELXL* runs as a function of dose.

individual anisotropic thermal displacement parameters (ADPs). Since the temperature was kept constant at 100 K during the experiment, the increase in the *B*-factors should be mainly caused by radiation-damage-induced structural disorder, *i.e.* an increase in the mosaicity.

It is well known that librational motion as described by ADPs can artificially change bond lengths (Busing & Levy, 1964). The libration correction can unfortunately only be calculated when the atomic components of molecular motion are understood. Since the ADPs model both vibration and disorder, one cannot, from an X-ray diffraction experiment alone, distinguish between the two effects. We decided to perform this correction irrespective of the effect causing the anisotropy of the ADPs in order to reach a qualitative conclusion of the significance of bond-distance changes. For the carbonyl C═O bonds, a libration of the carbonyl oxygen around the C atom can be assumed. A correction for such riding motion is implemented, *e.g.* in the program *XP* (Sheldrick, 1998), and we have applied a correction to the bond length for the C40—O40 bond exemplarily. Fig. 7 shows the possible bond distance alteration for a lower limit, for riding

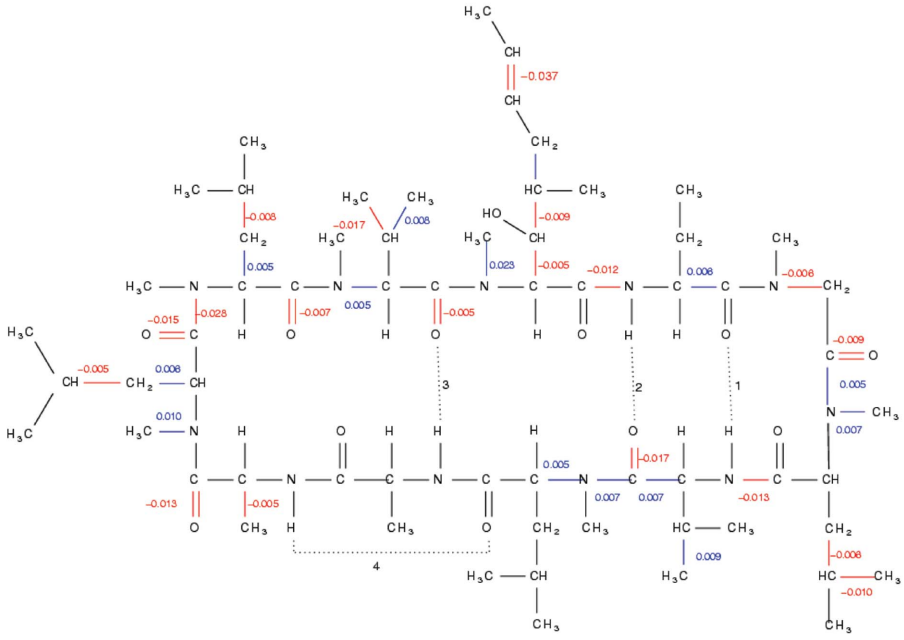

Figure 4
Chemical bond contractions (red) and elongations (blue) in cyclosporine A in Ångstroms between the first (2.3 MGy) and the last (69.1 MGy) data set. Only significant bond-length changes larger/smaller than +/− 0.0045 Å are shown.

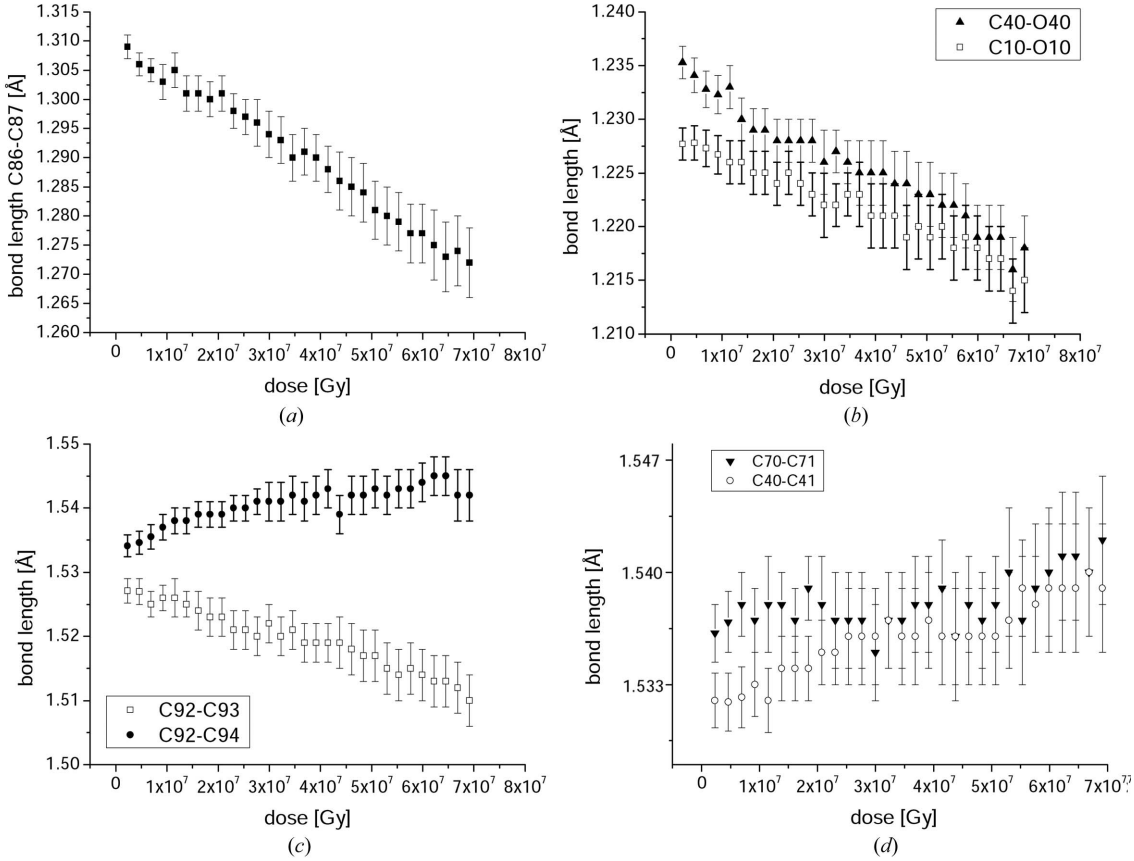

Figure 5
Selected bond-length changes including standard deviations as obtained from structure refinements as a function of dose. The small standard deviations compared with the absolute changes indicate the high significance of the changes. See Fig. 1 for atom name convention.

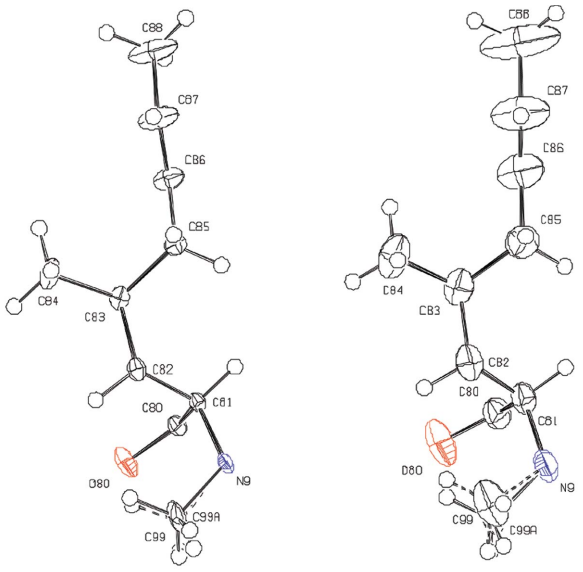

Figure 6
Thermal displacement ellipsoids of the C86—C87 atoms in their chemical environment at 2.3 MGy (left) and 69.1 MGy (right).

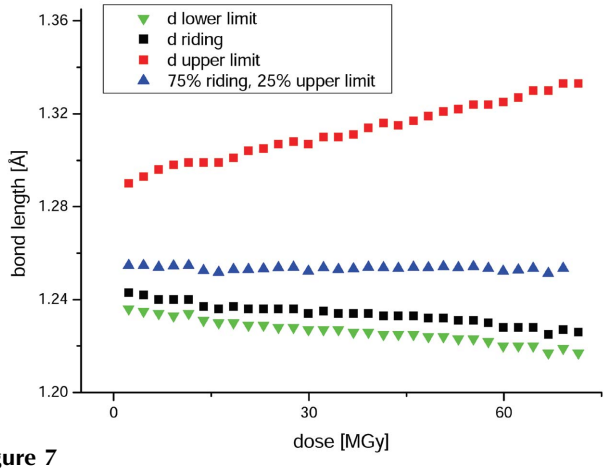

Figure 7
Effect of the ADPs on the bond distance of the C40—O40 bond as a function of dose for a lower limit, for riding motion and for an upper limit and a combination of 75% riding motion and 25% upper limit according to Busing & Levy (1964).

motion and for an upper limit as a function of dose for the C40—O40 bond. The bond-length contraction observed prevails assuming a 'lower limit' (term coined by Busing & Levy). Correcting the influence of the ADP increase on the bond length assuming a riding model, the bond still contracts, but less pronounced. The resulting curve for the upper limit looks similar to the increase in the relative *B*-factors (Fig. 2*c*) and would even allow for a bond elongation.

We can indeed achieve a constant bond length with increasing *B*-factors for this bond, by combining a 25% contribution from the 'upper limit' with a 75% contribution from the riding model (Fig. 7). Interestingly the individual percentage of the correction is different for each C=O bond and most of them still show a contraction even after a libration correction assuming riding motion. This indicates that the increase of ADPs is not only caused by misalignment of intact molecules owing to, for example, an increase in mosaicity, since if this were the case a similar behaviour for all carbonyl groups would be expected. Thus there must be a specific damage component to the molecules themselves.

4. Discussion

Our cyclosporine A crystal shows a typical response to irradiation with intense X-rays as has been described many times in the literature (Teng & Moffat, 2000; Ravelli *et al.*, 2002; Burmeister, 2000; Ravelli & McSweeney, 2000; Weik *et al.*, 2000; Müller *et al.*, 2002). The unit-cell volume, crystal mosaicity, lattice strain and relative *B*-factor all increase with increasing dose. At the same time the diffracted Bragg intensity, the correlation coefficients between the first and the subsequent data sets, and the agreement between the measured and model amplitudes (*R* value) each decrease with increasing dose.

In the structure refinements, specific bond-length changes are observed (Fig. 4). We would like to point out that an X-ray diffraction experiment averages over a very large number of unit cells. To influence the average bond length in a least-squares refinement, a substantial number of molecules must be affected. In the presence of radiation damage, the obtained bond length represents an average value between the damaged and undamaged state. Since the radiation-damage-induced increase of the ADPs can cause apparent bond contractions, care must be taken when chemically interpreting the changes in bond lengths with increasing *B*-factors. From this standpoint the observed phenomenon of bond-distance alterations can be understood as a radiation-induced chemical modification of the molecules leading to specific disorder as well as global disorder.

Cyclosporine A does not contain any carboxylic or sulfuric residues, which are known for their susceptibility to specific radiation damage. Thus another radiation damage mechanism must be responsible for the changes observed. A possible cause for both specific and global disorder could be radiation-induced hydrogen abstraction, which is a well known reaction in radiation chemistry (Cook & Whiffen, 1962; Lamvik *et al.*, 1983; Garrison, 1987). In the case of proteins and peptides, hydrogen abstraction from the α-carbon of the backbone is a well known radiolytic process (Garrison, 1987). In electron paramagnetic resonance (EPR) studies of γ-irradiated *n*-alkanes and branched alkanes at 77 K, hydrogen abstraction was mainly observed at penultimate C atoms. The susceptibility to hydrogen abstraction was found to be strongly dependent on the molecular environment, *e.g.* in the case of alkanes on the ability of performing a C—C—C bending motion (Ichikawa & Yoshida, 1992). Following this reasoning it is difficult to predict further possible positions of hydrogen abstraction of complex molecules such as cyclosporine A in addition to the α-C atoms, since little is known about the ability of different parts of the molecule to perform such bending motions in the crystalline state. Nevertheless, in the case of cyclosporine A, radiation-induced hydrogen abstraction could explain the specific structural changes observed in the aliphatic side chains. γ-Irradiation, electron irradiation

and VUV irradiation are already known for generating double bonds in polyethylene at doses of less than 2.5 MGy (Ungar, 1981; Waterman & Cole, 1971; Wilken *et al.*, 2002). The X-ray energy used in our experiment is in between the γ and VUV energy regime. Thus X-ray-induced double-bond formations in a statistic distribution of molecules in the cyclosporine A crystal might explain the bond contractions observed in the aliphatic side chains.

The mechanism of radiation-induced hydrogen abstraction in hydrocarbons can be explained by radiation-induced excitation of C—H and C—C bonds (Ungar, 1981, and references therein). According to Ungar, the C—H excitons are localized and thereby lead to an immediate break of the C—H bonds, either *via* direct scission or an ionic mechanism as suggested by other authors. In contrast to this, C—C excitons can move rapidly along the main chain resulting in only very few C—C ruptures. The C—C excitons can be trapped by defects in the chain such as double bonds by trapping positive charges. A positive hole trapping capability of *trans*-configured double bonds for C—C excitons might explain the large contraction observed for the C86═C87 double bond of cyclosporine A in this work. The binding energy of the resulting vinylene cation is slightly higher than for a double bond and hence a bond contraction is expected.

Further reactions of the primary hydrogen radicals H have been suggested by different authors (Ungar, 1981), *e.g.* the abstraction of another H atom. Common to most of them is formation of molecular hydrogen H_2 as the final reaction product.

In contrast to the $I/\sigma(I)$ ratio and the mean intensity which decay in an exponential manner with dose, the chemical bonds contract or elongate linearly with dose. A similar behaviour is observed for the decay of the correlation coefficient. Assuming chemical damage as the only causative of radiation damage, one would expect the same linear decay for the Bragg intensities as observed for the bond-lengths changes. Thus an additional process other than only chemical damage might be responsible for the loss of crystalline order of the sample as observed by increased crystal mosaicity and the unit-cell volume. Assuming hydrogen abstraction is taking place, the resulting gaseous hydrogen might deteriorate the crystalline order in an unfavourable manner. Such a formation of gaseous hydrogen bubbles upon intense electron irradiation is well known in electron microscopy (Leapman & Sun, 1995).

5. Conclusion and outlook

We suspect that radiation-induced hydrogen abstraction could explain the structural changes observed. The subsequent formation of hydrogen gas inside the crystal would also explain the frequently observed increase of the crystal mosaicity and hence the increase in *B*-factors.

These findings were obtained from a peptide crystal possessing a very low solvent content; thus the process of hydrogen abstraction is probably not a water-mediated process. Conversely, to our knowledge there is no mechanism by which water could suppress this process. Thus, we expect hydrogen abstraction also to take place in macromolecular crystals possessing much higher solvent contents.

Further EPR and neutron diffraction experiments on pre-damaged crystals are necessary to fully understand the process of radical formation and the structural changes observed in this work. The combination of X-ray crystallography with *in situ* Raman or *in situ* IR spectroscopy at cryogenic temperatures might also be useful to characterize bond-length alterations.

We thank Dr S. Dechert for discussions about Raman spectroscopy and Dr W. Morgenroth for his helpful comments. SG was supported by the NCCR Structural Biology program of the Swiss National Science Foundation. BD thanks the DFG for funding (Di921/3-1). We would also like to thank the referees for their helpful suggestions, time and effort.

References

Burmeister, W. P. (2000). *Acta Cryst.* D**56**, 328–341.
Busing, W. R. & Levy, H. A. (1964). *Acta Cryst.* **17**, 142–146.
Comolli, L. R. & Downing, K. H. (2005). *J. Struct. Biol.* **152**, 149–156.
Cook, R. J. & Whiffen, D. H. (1962). *Phys. Med. Biol.* **7**, 277–300.
Dubochet, J. (1988). *Q. Rev. Biophys.* **21**, 129–228.
Garrison, W. M. (1987). *Chem. Rev.* **87**, 381–398.
Giron, D., List, M., Richter, F., Uike, Y. & Weber, H. P. (1989). De 38 43 054 c2. Deutsches Patent- und Markenamt, Patentinhaber: Novartis AG, Basel, Switzerland.
Ichikawa, T. & Yoshida, H. (1992). *J. Phys. Chem.* **96**, 7656–7661.
Johnas, S., Dittrich, B., Meents, A., Messerschmidt, M. & Weckert, E. (2009). *Acta Cryst.* D**65**. In the press.
Kabsch, W. (1993). *J. Appl. Cryst.* **26**, 795–800.
Lamvik, M. K., Kopf, D. A. & Robertson, J. D. (1983). *Nature (London)*, **301**, 332–334.
Leapman, R. D. & Sun, S. (1995). *Ultramicroscopy*, **59**, 71–79.
Luedeke, A. (2004). *Proceedings of the 9th Biennial European Particle Accelerator Conference (EPAC 2004)*, Lucerne, Switzerland, pp. 2281–2283.
Müller, R., Weckert, E., Zellner, J. & Drakopoulos, M. (2002). *J. Synchrotron Rad.* **9**, 368–374.
Murray, J. W., Rudiño-Piñera, E., Owen, R. L., Grininger, M., Ravelli, R. B. G. & Garman, E. F. (2005). *J. Synchrotron Rad.* **12**, 268–275.
Owen, R. L., Holton, J. M., Schulze-Briese, C. & Garman, E. F. (2009). *J. Synchrotron Rad.* **16**, 143–151.
Ravelli, R. B. G. & McSweeney, S. M. (2000). *Structure*, **8**, 315–328.
Ravelli, R. B. G., Theveneau, P., McSweeney, S. & Caffrey, M. (2002). *J. Synchrotron Rad.* **9**, 355–360.
Schulze-Briese, C., Ketterer, B., Pradervand, C., Bronnimann, C., David, C., Horisberger, R., Puig-Molina, A. & Graafsma, H. (2001). *Nucl. Instrum. Methods Phys. Res. A*, **467–468**, 230–234.
Sheldrick, G. M. (1998). *XP*. Bruker AXS, Madison, WI, USA.
Sheldrick, G. M. (2008). *Acta Cryst.* A**64**, 112–122.
Stark, H., Zemlin, F. & Boettcher, C. (1996). *Ultramicroscopy*, **63**, 75–79.
Symons, M. C. R. (1982). *Ultramicroscopy*, **10**, 97–103.
Teng, T. & Moffat, K. (2000). *J. Synchrotron Rad.* **7**, 313–317.
Tong, L. (2001). *International Tables for Crystallography*, Volume F, edited by M. G. Rossmann and E. Arnold, pp. 275. Dordrecht: Kluwer.
Ungar, G. (1981). *J. Mater. Sci.* **16**, 2635–2656.
Waterman, D. C. & Cole, M. (1971). *J. Phys. Chem.* **75**, 3988–3992.
Weik, M., Ravelli, R. B. G., Kryger, G., McSweeney, S., Raves, M. L., Harel, M., Gros, P., Silman, I., Kroon, J. & Sussman, J. L. (2000). *Proc. Natl Acad. Sci. USA*, **97**, 623–628.
Wilken, R., Holländer, A. & Behnisch, J. (2002). *Plasm. Polym.* **7**, 19–39.